Journal Name

COMMUNICATION

Trapping Shape-Controlled Nanoparticle Nucleation and Growth Stages via Continuous-Flow Chemistry

Received 00th January 20xx,
Accepted 00th January 20xx

DOI: 10.1039/x0xx00000x

www.rsc.org/

Alec P. LaGrow,*[ad] Tabot M. D. Besong,[a] Noktan M. AlYami,[a] Khabiboulakh Katsiev,[b] Dalaver H. Anjum,[c] Ahmed Abd Elkader,[a] Pedro M. F. J. Costa,[a] Victor M. Burlakov,[e] Alain Goriely[e] and Osman M. Bakr*[a]

Continuous flow chemistry is used to trap the nucleation and growth stages of platinum-nickel nano-octahedra with second time resolution and high throughputs to probe their properties *ex-situ*. The growth starts from poorly crystalline particles (nucleation) at 5 seconds, to crystalline 1.5 nm particles bounded by the {111}-facets at 7.5 seconds, followed by truncation and further growth to octahedral nanoparticles at 20 seconds.

Nanoparticles have become ubiquitous in the literature for their applications, in catalysis,[1] magnetism,[2,3] biomedicine[2,3] and optics.[1,2] Solution synthesis techniques for nanoparticles have rapidly increased in sophistication, with a library of sizes and shapes being generated.[4] However, controlling the growth of nanoparticles is still more of an art due to the lack of techniques that can probe the initial stages of nanoparticle growth with the necessary time resolution and sensitivity.[4,5] For shape-controlled nanoparticles syntheses, it is typically considered that initial nuclei grow into a seed crystal that controls the growth into the final shaped nanoparticle.[4] However, direct evidence for the identity of the initial nuclei and how faceting develops have not been experimentally shown. The insensitivity of in-situ techniques to the formation of defects and crystal facets is a major barrier for obtaining such evidence.[6,7]

Due to the above-mentioned limitations, ex-situ techniques dominate the discussion of nanoparticle growth by taking aliquots, or quenching the reaction at certain intervals.[8,9] However, the initial nucleation step of the nanoparticle synthesis can occur within seconds[7,10,11] of the start of the reaction and in very low yields.[12] This restricts the use of aliquots to study nucleation as their time resolution is limited by the heat transport of the reaction solution, the amount of aliquot needed and the ease and frequency with which the aliquot is acquired.

Here-in, we use a continuous flow reactor[11,13-15] to precisely control the reaction time to selectively trap the nucleation and growth stages. The use of millifluidics allows access to a heat transfer coefficient orders of magnitude higher than typical batch reactions, and therefore allows the reaction to be initiated and quenched in fractions of a second without the need of introducing a foreign agent (e.g., quenching chemical) to the reaction. By using high angle annular dark field scanning transmission electron microscopy (HAADF-STEM) and analytical ultracentrifugation (AUC), we were able to detect and observe the particle growth starting from disordered clusters of atoms, to {111} dominated crystals, of 1.5 nm in size, that grow into fully formed octahedral nanoparticles. Due to the continuous nature of the synthesis, every stage in the reaction could be isolated in a large scale.[14,16]

[a] King Abdullah University of Science and Technology (KAUST), Division of Physical Sciences and Engineering (PSE), Thuwal 23955-6900, Saudi Arabia.
[b] King Abdullah University of Science and Technology (KAUST), SABIC Corporate Research and Innovation Center, Thuwal, 23955-6900, Saudi Arabia.
[c] King Abdullah University of Science and Technology (KAUST), Imaging and Characterization Lab, Thuwal 23955-6900, Saudi Arabia.
[d] York Nanocentre, University of York, Heslington, York YO10 5DD, U.K.
[e] Mathematical Institute, University of Oxford, Oxford OX2 6GG, U.K.
Electronic Supplementary Information (ESI) available: See DOI: 10.1039/x0xx00000x

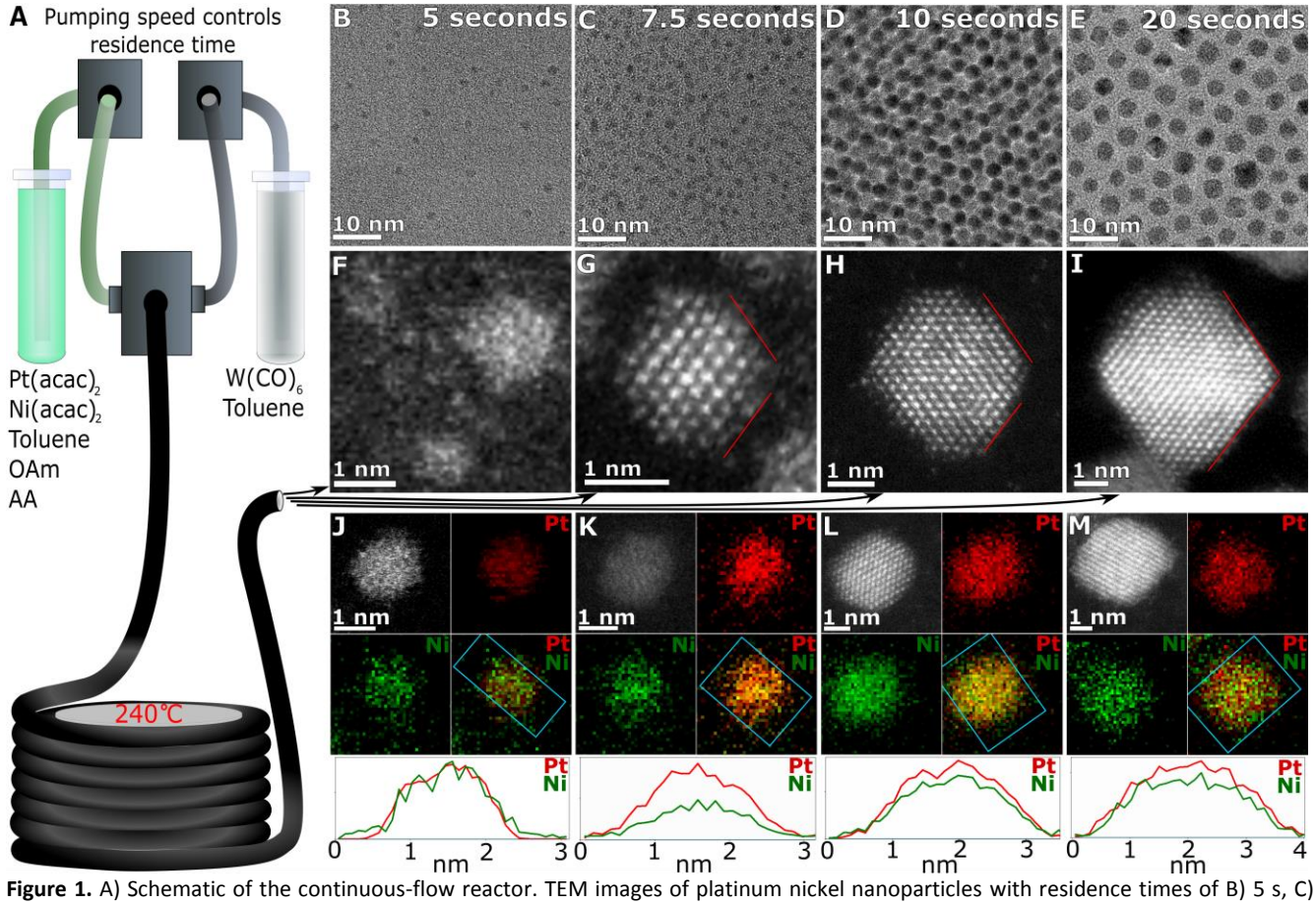

Figure 1. A) Schematic of the continuous-flow reactor. TEM images of platinum nickel nanoparticles with residence times of B) 5 s, C) 7.5 s, D) 10 s and E) 20 s and HAADF-STEM images of F-I) respectively. The red lines indicate the {111} facet (Fig. S8). STEM-EELS spectrum imaging of a J) amorphous, K) ~1.5 nm, L) ~2.5 nm and M) ~3.3 nm particle. The line profiles below (J-M) are from the blue

The growth of platinum-nickel (Pt-Ni) nanooctahedra was studied by quenching the reaction with second intervals in a continuous-flow reactor.[16, 17] The reaction was carried out with surfactants, oleylamine (OAm) and 1-adamantane carboxylic acid (AA), and a source of carbon monoxide, tungsten carbonyl [$W(CO)_6$]. The $W(CO)_6$ acts as a source of CO and the tungsten remains in solution in a partially oxidized form (Fig. S1). Platinum acetylacetonate [$Pt(acac)_2$] and nickel acetylacetonate dihydrate [$Ni(acac)_2.2H_2O$] were used as precursors at 240°C in toluene. The reaction was run continuously with residence times of 5, 7.5, 10, and 20 seconds (Fig. 1A). The HAADF-STEM was taken from the first frame exposed to the beam (Fig. S2-S4). With the 5 second residence time, the formation of 1.3 ± 0.3 nm particles of ~$Pt_{72}Ni_{28}$ with a large proportion of ~1.3 nm crystalline particles, disordered particles of ≤1 nm and loose single atoms were observed (Fig. 1B, F, Fig. S5 and Table S1). The same species as at 5 seconds were seen at times shorter than 5 seconds but with much lower yields. With a residence time of 7.5 seconds crystalline particles of 1.5 ± 0.2 nm ~$Pt_{82}Ni_{18}$ were formed with the {111}-facets exposed on the surface (Fig. 1C, G and Fig. S6). With a 10 second residence time, 2.6 ± 0.4 nm cuboctahedral particles of ~$Pt_{54}Ni_{46}$ were formed (Fig. 1D, H, Table S1 and Fig. S7). With a 20 second residence time, nanooctahedra of ~$Pt_{47}Ni_{53}$ (3.6 ± 0.5 nm) were formed (Fig. 1E, I and Table S1).

STEM-electron energy loss spectroscopy (EELS) spectrum imaging of an amorphous particle showed nearly equal proportions of Pt:Ni (Fig. 1J). The ~1.5 nm crystalline particle was platinum rich (Fig. 1K), while the larger ~2.5 and ~3.3 nm particles tended towards parity with time (Fig. 1L and M). In each particle the platinum and nickel signals matched each other, showing that the particles formed a random alloy structure (Fig. 1J-M). X-ray diffraction of the nanoparticles show a decrease in lattice parameters and sharpening of peaks with increased residence time, consistent with the nickel enrichment of the alloy and an increase in particle size (Fig. S9 and Table S2).

Theoretical analysis of the nanoparticle growth stages carried out in SI section 3 indicate that the process of nucleation and growth in this system occurs initially to minimize its surface energy. As the particle grows, it crystallizes and becomes dominated by the exposure of energetically favorable low index facets, namely the lowest energy {111}-facets (SI section 3),[19] which is also chemically favored by the addition of CO.[18,20] The particles initially crystallize with predominantly platinum atoms due to the higher cohesive energy of platinum compared to nickel, causing the detachment rate of nickel atoms to be higher than that of platinum (SI section 3).[21] As the particles grow, the platinum to nickel ratio tends towards parity as the platinum is

initially depleted from the solution and the nickel becomes the major additive, and therefore dominates the chemistry.

Analytical ultracentrifugation (AUC) is used to analyze distinct species in solution from the nanoparticle systems.[22]

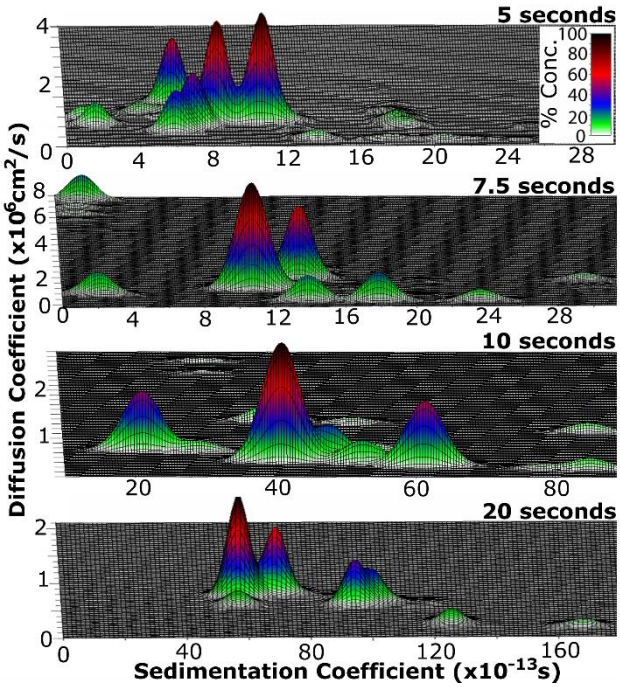

The AUC indicates an increase in the sedimentation coefficient and corresponding hydrodynamic diameter of the nanoparticles with increasing residence times in the flow reactor (Fig. 2, Fig S10, S11 and Table S3-S8). During the nucleation step there are five major components present (5 seconds, Fig. 2) which decreases to only two major species present in the 7.5 second sample (Fig. 2). The major peak in the 5 and 7.5 second samples have a similar peak position and would correspond to the crystalline particles of ~1.3 nm (Fig. 2). The species at the lowest sedimentation coefficients are expected to be from the precursor and reduced monomers, they are seen in the samples with residence times of 5 and 7.5 seconds but are no longer present with a residence time of 10 seconds (Fig. 2). In the 10 second sample the major species are at much higher sedimentation coefficients and a distribution of the smaller species is observed (Fig. 2). The 20 second sample only contained the larger species, which are expected to be the octahedral nanoparticles (Fig. 2).

Figure 2. 3-D representation of the relative concentrations, sedimentation and diffusion coefficients from AUC at 5-20 s.

To determine the ligand shell surrounding the nanoparticles, fourier transform infrared spectroscopy (FTIR) and x-ray photoelectron spectroscopy (XPS) was utilized. The FTIR spectra of all samples had three peaks from 2850 – 2960 cm^{-1} which would correspond to aliphatic CH_2 stretches. The FTIR spectrum for the 5 second sample had an O-H stretch at 3227 cm^{-1}, and stretches at 1300-1000 cm^{-1} indicative of a C-O stretch (Fig. S12). These could come from the reduced acetylacetonate. The 7.5-second sample had a large stretch at 1697 cm^{-1} indicating an unbound C=O stretch which is attributed to either the acetylacetonate or the adamantine carboxylic acid (Fig. S12). For the 10 second sample, the FTIR spectrum has an N-H bond at 1633 cm^{-1}, indicating the presence of oleylamine on the surface. The lack of the N-H stretch around 3300 cm^{-1} is due to the amine moiety binding to the metal surface.[23] For, the 20 second sample, the FTIR spectrum has a mixed ligand environment with carbonyl and amine groups (Fig. S12).

The XPS of the nitrogen has two components in the samples. The first component at ~400 eV corresponded to C-NH_2 (Fig. S13 and Table S9). The second component can be seen at 399 eV up till the 10 second sample and then at 398 eV in the 20 second sample (Fig. S13 and Table S9). The peak at 398 eV would be a strong M-N bond as reported with Pt-N.[24] The peak at 399 eV could be due to a weaker M-N bond or a distorted ligand environment, it is observed to shift to lower energy and increase in proportion with longer residence times. For Pt and Ni, the dominant signal is reduced metal (Fig. S13 and Table S9).

From the combination of the STEM, AUC, FTIR and XPS results, we show that the initial nucleation of particles occurs in the formation of low crystallinity metallic platinum-nickel clusters of atoms of multiple sizes that are surrounded by acetylacetonate ligands (Fig. 3). Within seconds, platinum rich crystalline particles of 1.3 nm and above form and are predominantly bound by the {111} facets, the size distribution narrows, by 7.5 seconds, while continued nucleation is still occurring. As growth progresses, the nanoparticle size increases as the dominant mechanism in the reaction favors nanoparticle growth (after 10 seconds), and the acetylacetonate ligand environment decomposes[6] and is replaced by loosely bound amine ligands as confirmed by FTIR and XPS results (Fig. 3). The nickel that was left in solution adds to the nanoparticles, dominating the surface chemistry of the particles and adding preferentially on the {111} facets, due to the presence of carbon monoxide.[18,20] Growth slows down as last of the nickel is incorporated into the alloy structure and the strong M-N bond forms with the amine surfactants (after 20 seconds) which stabilize the particles from aggregation[23] as well as reduce the addition rate of incoming atoms to the particles surface.[25]

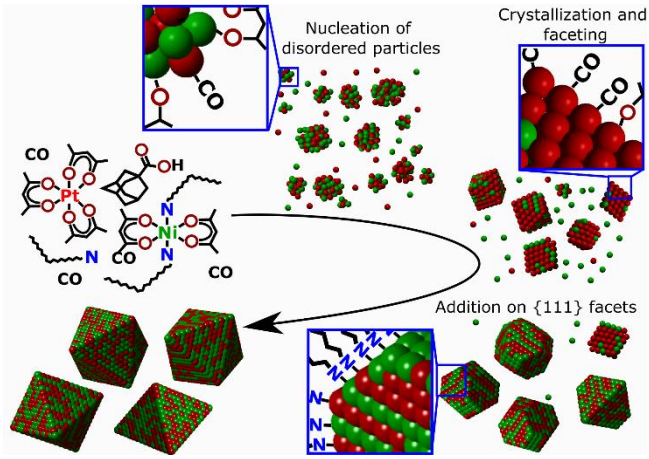

Figure 3. Growth mechanism schematic.

To study the properties of particles in the trapped stages, it is necessary to establish the particles stability both *ex situ* and in solution. The nuclei were stable once quenched and could be stored in toluene for over 6 months without noticeable changes in the size distributions measured by TEM or AUC. The ultra-small particles were also seen to be thermally stable under ultrahigh vacuum conditions up to 1100°C if they are physically separated (Fig. S14 - S17), or up to 600°C if they are not (Fig. S13 and S15). The particles also show reasonable facet stability up to 1100°C (Fig. S14 - S16). For the 1.5 nm particles Ostwald ripening was observed (Fig. S17). The facet stability is attributed to the thermal stability of the {111} surface facet.[26] The 5 second sample species are seen to be stable up to 1100°C and still show populations of single atoms, disordered and crystalline particles (Fig. S18). The trapped particles were stable once quenched and therefore could be utilized in a wide range of applications.

Both pure platinum and platinum alloys were investigated under the conditions described above, at 240°C with oleylamine, adamantine carboxylic acid and $W(CO)_6$. The pure platinum particles were observed with a 5 second residence time forming smaller clusters and bigger cuboctahedra with an average size of 1.4 ± 0.7 nm (Fig. 4A and Fig. S19), which became 7 ± 2 nm cubes after 7.5 minutes (Fig. 3B). For platinum-copper, the particles were seen to be 0.9 ± 0.2 nm ~$Pt_{25}Cu_{75}$ after 10 seconds (Fig. 4C and Fig. S19) and 3.5± 0.7

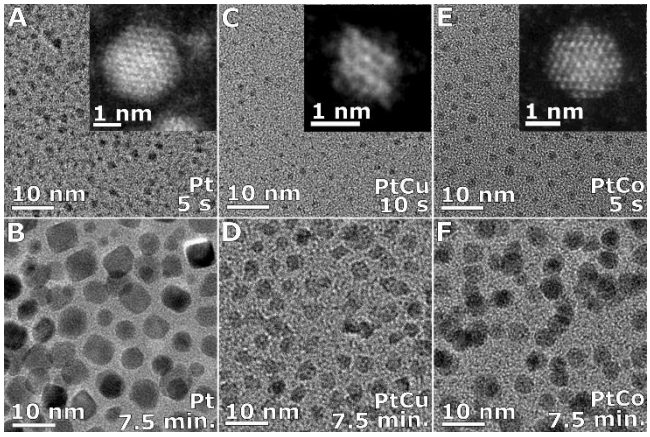

Figure 4. TEM images of platinum at A) 5 s and B) 7.5 min., platinum copper at C) 10 s and D) 7.5 min., and platinum cobalt at E) 5 s and F) 7.5 min.

nm ~$Pt_{60}Cu_{40}$ octahedra after 7.5 minutes (Fig. 4D and Fig. S20). Platinum-cobalt with a residence time of 5 seconds formed ~$Pt_{91}Co_9$ truncated cuboctahedra of 1.7 ± 0.3 nm (Fig. 4E**,** Fig. S19 and Fig. S20), which became 4.4 ± 0.7 nm ~$Pt_{70}Co_{30}$ cuboctahedra after 7.5 minutes (Fig. 4F and Fig. S20).

In the case of pure platinum the {100}-facets on the particle's surface does not occur until larger sizes, in agreement with the literature.[27] For the platinum cobalt alloys, the initial formation of platinum rich seeds followed by the addition of the less noble metal and its subsequent alloying into the structure, indicates that the less noble metal dominates the shape control.

To apply the trapping procedure to a range of materials, several parameters must be considered. The reducing agent must not cause reduction at low temperatures allowing the temperature to activate and quench the reaction, making it ideal for weak reducing agents used in many shape controlled syntheses. The formed particles must be stable once quenched.

In summary, this study reports the use of continuous-flow chemistry to trap the stages of nucleation and growth with a resolution of seconds. The investigation of the growth of platinum-nickel nano-octahedra demonstrates the initial formation of disordered clusters of various sizes that crystallize into monodisperse single crystalline platinum-rich particles with the {111} crystal facet on the surface. The initially platinum-rich nanoparticles increase their nickel content as the octahedral shape of the particles evolve. The ligand shell of the particles transformed from the ligand shell of the precursor, at 5 seconds, to the amine surfactant as the particles grew to completion. The synthetic technique was applied to platinum, and platinum alloys and shows broad applicability. The methodology demonstrated in this work paves the way to study the nucleation and growth stages of a wide range of nanoparticulate systems.

The research reported in this publication was supported by funding from KAUST. APL and OMB designed the experiments. The syntheses were carried out by APL, NMA and DTB. TEM was carried out by APL, DHA and NMA. STEM-EELS maps were carried out by DHA. AUC and FTIR was carried out by DTB, XRD by NMA, and XPS by KhK. In-situ heating was carried out by APL, AAE and PMFJC. Theory was carried out by VMB and AG. All authors contributed to the production of the manuscript.

References

1 C. Burda, X. B. Chen, R. Narayanan and M. A. El-Sayed, *Chem. Rev.*, 2005, **105**, 1025-1102.
2 B. H. Kim, M. J. Hackett, J. Park and T. Hyeon, *Chem. Mater.*, 2013, **26**, 59-71.
3 J. Gao, H. Gu and B. Xu, *Acc. Chem. Res.*, 2009, **42**, 1097-1107.
4 Y. Xia, Y. Xiong, B. Lim and S. E. Skrabalak, *Angew. Chem. Int. Ed.*, 2009, **48**, 60-103.
5 M. V. Kovalenko, L. Manna, A. Cabot, Z. Hens, D. V. Talapin, C. R. Kagan, V. I. Klimov, A. L. Rogach, P. Reiss, D. J. Milliron, P. Guyot-Sionnnest, G. Konstantatos, W. J. Parak, T. Hyeon, B. A. Korgel, C. B. Murray and W. Heiss, *ACS Nano*, 2015, **9**, 1012-1057.
6 A. P. LaGrow, B. Ingham, M. F. Toney and R. D. Tilley, *J. Phys. Chem. C*, 2013, **117**, 16709-16718.
7 C. R. Bullen and P. Mulvaney, *Nano Lett.*, 2004, **4**, 2303-2307.
8 L. Gan, C. Cui, M. Heggen, F. Dionigi, S. Rudi and P. Strasser, *Science*, 2014, **346**, 1502-1506.
9 M. R. Langille, M. L. Personick, J. Zhang and C. A. Mirkin, *J. Am. Chem. Soc.*, 2012, **134**, 14542-14554.
10 I. Lignos, S. Stavrakis, A. Kilaj and A. J. deMello, *Small*, 2015, **11**, 4009-4017.
11 V. Sebastian and K. F. Jensen, *Nanoscale*, 2016, **8**, 15288-15295.
12 M. A. Watzky and R. G. Finke, *J. Am. Chem. Soc.*, 1997, **119**, 10382-10400.

13 J. Pan, A. a. O. El-Ballouli, L. Rollny, O. Voznyy, V. M. Burlakov, A. Goriely, E. H. Sargent and O. M. Bakr, *ACS Nano*, 2013, **7**, 10158-10166.
14 H. Mehenni, L. Sinatra, R. Mahfouz, K. Katsiev and O. M. Bakr, *RSC Adv.*, 2013, **3**, 22397-22403.
15 N. M. AlYami, A. Lagrow, k. Joya, J. Hwang, K. Katsiev, D. H. Anjum, Y. Losovyj, L. Sinatra, J. Y. Kim and O. M. Bakr, *Phys. Chem. Chem. Phys.*, 2016, **18**, 16169-16178.
16 S. E. Skrabalak and R. L. Brutchey, *Chem. Mater.*, 2016, **28**, 1003-1005.
17 A. P. LaGrow, K. R. Knudsen, N. M. AlYami, D. H. Anjum and O. M. Bakr, *Chem. Mater.*, 2015, **27**, 4134-4141.
18 J. Zhang, H. Yang, J. Fang and S. Zou, *Nano Lett.*, 2010, **10**, 638-644.
19 L. Vitos, A. V. Ruban, H. L. Skriver and J. Kollár, *Surf. Sci.*, 1998, **411**, 186-202.
20 S. Y. Hwang, M. Zhang, C. Zhang, B. Ma, J. Zheng and Z. Peng, *Chem. Commun.*, 2014, **50**, 14013-14016.
21 V. M. Burlakov and L. Kantorovich, *J. Chem. Phys.*, 2011, **134**, 024521.
22 R. P. Carney, J. Y. Kim, H. Qian, R. Jin, H. Mehenni, F. Stellacci and O. M. Bakr, *Nat. Commun.*, 2011, **2**, 335.
23 J. Zhang and J. Fang, *J. Am. Chem. Soc.*, 2009, **131**, 18543-18547.
24 X. Li, L. An, X. Chen, N. Zhang, D. Xia, W. Huang, W. Chu and Z. Wu, *Scientific Reports*, 2013, **3**, 3234.
25 A. M. Karim, N. Al Hasan, S. Ivanov, S. Siefert, R. T. Kelly, N. G. Hallfors, A. Benavidez, L. Kovarik, A. Jenkins, R. E. Winans and A. K. Datye, *J. Phys. Chem. C*, 2015, **119**, 13257-13267.
26 Y. Wen, H. Fang, Z. Zhu and S. Sun, *Phys. Lett. A*, 2009, **373**, 272-276.
27 H.-G. Liao, D. Zherebetskyy, H. Xin, C. Czarnik, P. Ercius, H. Elmlund, M. Pan, L.-W. Wang and H. Zheng, *Science*, 2014, **345**, 916-919.